A Simplified Predictive Current Control of Open-End Winding Permanent Magnet Synchronous Motor

Sagar Gajanan Petkar and Vinay Kumar Thippiripati, *Senior Member, IEEE*

***Abstract*—Model predictive current control (MPCC) of a 4-level inversion fed open-end winding permanent magnet synchronous motor (OEW-PMSM) using 37 voltage vectors (VV) suffers from the disadvantage of the increased computation burden. A high computation burden on the processor puts a limit on the selection of the minimum sampling time. In this article, a novel method is presented for reducing the computation burden. The proposed method reduces the number of candidate VVs from 37 to a maximum of 4 and a simple cost function is proposed to select the optimal VV. The proposed method calculates the change in stator current (CSC) needed to obtain the required change in the stator flux. The CSC vector is in the direction of the required change in the stator flux, which is used to shortlist the candidate VV for the reduced control set. The required change in the flux is obtained using the reference stator current of the next sample. The multiple predictions of the *d-q* currents are eliminated and a simple cost function based on the difference between per-unit CSC and candidate VV is used to simplify the calculations. The proposed method is experimentally tested and compared with existing MPCC. The results confirm the effectiveness of the proposed scheme.**

***Index Terms*—Permanent magnet synchronous motor drive, predictive current control.**

I. Introduction

PERMANENT magnet synchronous motor (PMSM) has wide industrial applications due to multiple merits like high power density, simple structure, high efficiency, and wide speed range [1], [2], [3], [4]. The power delivered by the PMSM would be restricted owing to the inverter power handling capacity. This deficiency is overcome with the introduction of the open-end winding configuration of PMSM (OEW-PMSM). The OEW-PMSM is achieved by opening the neutral point of the PMSM and connecting a second inverter across it [5]. The stator winding of OEW-PMSM is supplied simultaneously by both the inverters connected on two sides. This doubles the power capacity of the PMSM system and can be conveniently used in high-power applications [6]. Also, the OEW-PMSM is characterized by the multilevel phase voltage, which leads to precise torque control and fewer harmonics in the stator current [7]. The OEW-PMSM drive can be classified into two types depending on whether the dc voltage sources used for two inverters are common or separate, i.e., OEW-PMSM drives with a common dc voltage source [8] and OEW-PMSM with an isolated dc voltage source [9]. In OEW-PMSM with isolated dc voltage sources, different multilevel voltage effects can be achieved by selecting the proper ratio of dc link voltages [10]. This arrangement of two isolated dc voltage sources makes the drive more complex and costlier. In OEW-PMSM with a common dc source, both the inverters share the same dc voltage source and the drive requires only one dc voltage source. In this configuration, a zero-sequence loop is inherently present due to a direct connection between two inverters with a common dc link [11]. This would result in zero-sequence current (ZSC) to flow in the zero-sequence loop under the presence of zero-sequence voltage. The most commonly used configurations of OEW-PMSM are three-level and four-level inversion fed OEW-PMSM. A 3-level inversion fed OEW-PMSM uses 19 voltage vectors (VV) that are produced through different switching conditions and with equal dc-link voltages of the dual inverters. The 4-level inversion fed OEW-PMSM uses 37 voltage vectors which are produced by the dual-inverters with dc link voltages in a ratio of 2:1.

Direct torque control (DTC) is a simple and popular control method for the PMSM drive. However, DTC suffers several drawbacks like high ripples in the torque and stator flux. Recent advancements in digital signal processors have started the extensive use of model predictive control (MPC) methods for obtaining the elevated performance of PMSM [12]. MPC has several merits like a fast response, high accuracy, and simple structure. Based on the control variables, MPC is classified into model predictive torque control (MPTC) and model predictive current control (MPCC) [13]. MPCC is simpler as compared to MPTC and does not involve any weighting factor in the cost function thereby eliminating the problem of the tuning of the weighting factor. The application of MPCC to three-level and four-level inversion fed OEW-PMSM drive involves the prediction of stator currents for every available VV during each sampling interval. The predictions of stator currents for a four-level OEW-PMSM are complex and put a huge computation burden on the digital processor.

Siami et al. [14] presented a computationally efficient MPC of a matrix converter fed PMSM drive to reduce the prediction VVs from 25 to 10. In [14], a look-up table is proposed to reduce the count of VVs. The proposed look-up table in [14] uses the position of the input VV, the direction of the stator flux

Manuscript received 6 April 2022; revised 19 July 2022; accepted 18 August 2022. Date of publication 24 August 2022; date of current version 10 October 2022. This work was supported in part by the Science and Engineering Research Board-Department of Science & Technology under Grant EEQ/2020/000072 and in part by the National Institute of Technology, Warangal, India. Recommended for publication by Associate Editor Z. Zhang. *(Corresponding author: Sagar Gajanan Petkar.)*

The authors are with the Electrical Engineering Department, National Institute of Technology, Warangal, Warangal 506004, India (e-mail: sagr.petkar@gmail.com; tvinay.nitw@gmail.com).

Color versions of one or more figures in this article are available at https://doi.org/10.1109/TPEL.2022.3201337.

Digital Object Identifier 10.1109/TPEL.2022.3201337

vector, and the torque demand. The method presented in [14] has reduced the computation burden by 40%. In [15], the branch and bound method is proposed to reduce the execution time of the MPTC-operated PMSM drive. The technique presented in [15] enables the use of MPTC over a long prediction horizon to improve the steady-state response of the PMSM drive.

The predictive torque control of a five-phase induction motor drive using selective VVs is presented in [16]. The control performance in [16] is the same as that of the conventional MPTC of a five-phase induction motor. The control set of the VVs is reduced by using the sector information of the stator flux vector and the torque error. As the VVs in the control set are reduced from 32 to 16, there is a considerable reduction in the computation time of the MPTC algorithm. A novel MPCC of the open-end winding induction motor drive in the A-B-C reference frame is presented in [17] for improving the algorithm complexity. The open-end winding induction motor in [17] has used dual inverters with a common dc-link. In this method, the reference currents in the A-B-C reference frame are found. The stator currents in the A-B-C frame for the next sampling instant are predicted with the possible stator phase voltage as $+V_{\mathrm{DC}}$, 0 or $-V_{\mathrm{DC}}$. The method presented in [17] has successfully reduced the computation burden on the controller through the reduction in the total number of predictions from 27 to 9. This method has also suppressed the zero-sequence current in the motor.

A simplified MPTC of four-level inversion fed open-end winding induction motor drive to alleviate the computation time is presented in [18]. The shortlisting of the VV is based on the nearest VV selection. A total of 12 VVs nearer to the optimal VV of the previous sample are shortlisted to form a reduced control set. The technique presented in [18] has shortlisted the VVs in the control set from 37 to 12. The shortlisting of the VVs has reduced 25 prediction calculations in every sampling interval. This method has reduced the computation burden by 43%. Authors in [19] have presented a less complex deadbeat MPCC of OEW-PMSM drive with ZSC suppression. In [19], the components of a reference VV are found based on the deadbeat theory. A reduced control set of candidate VVs is formulated by using the components of the reference VV. A VV present in the control set and matching the reference vector is selected as an optimal vector based on the optimization criteria. This method has considerably reduced the computation burden on the controller.

Luo and Liu [20] have proposed a less complex model of predictive flux control for a six-phase PMSM. In [20], a look-up table is used to exclude useless VVs for reducing the computation burden. The look-up table uses the sector number in which the flux vector is located along with the torque error, which is the difference between the reference torque and the actual torque. The computation time with [20] is reduced by 28.3%. An indirect reference VV-based MPC method is proposed in [21] for reducing the computation burden of the model predictive controlled PMSM drive. In [21], instead of calculating the reference VV in the traditional manner, the reference vector is found using two two-level hysteresis comparators. The complex α-β plane is divided into six triangular regions. The six VVs are selected for the predictions which are present in the same region as the reference vector.

A computationally efficient and simple weighting factor less MPTC of two-level inverter fed induction motor is proposed in [22]. Based on the previous VV, a group of four VVs is selected for the predictions. The predictions and evaluation of cost function are reduced from seven per sample to four per sample, thereby causing a 5% reduction in the computation burden. The improved MPC schemes of PMSM with better response are presented in [23], [24], and [25]. In the presented MPC methods [23], [24], [25], there is a reduction in the computation burden along with the reduced ripple in the torque. The motivation for this article is to further reduce the computation burden in a four-level OEW-PMSM drive.

This article proposes a technique for reducing the heavy computation burden in a four-level inversion fed MPCC of OEW-PMSM drive. The proposed technique in this article reduces the existing control set of 37 VVs and forms a further shorter control set which includes a maximum 4 VVs. A space vector of the required change in stator current (CSC) is calculated from the predicted current of the next sample, which is obtained from the speed proportional-integral (PI) controller. The complex $\alpha\beta$-plane is divided into 12 equal sectors and each sector is split into 3 zones. The sector number and the zone number are found in which the required CSC vector is located. Both the sector number and zone number are used for deciding the candidate VVs of the reduced control set. The per-unit candidate VV in the reduced control set, which is nearer to the per-unit required CSC vector, produces the change in the stator flux needed to achieve the predicted current. Therefore, this VV is selected as an optimal VV for the next sampling interval. The proposed method of this article decides the optimal VV without multiple predictions of the stator currents corresponding to each candidate VV. The absence of multiple predictions and a considerable reduction in the count of candidate VVs of the control set contributes to the reduction in the number of arithmetic operations, thereby reducing the computation time. The major contributions to this article are indicated in the following.

1) Unlike the existing methods which are based on the reference voltage calculation for reducing the calculation efforts, the proposed method calculates the required CSC vector for shortlisting the VVs. The proposed scheme is simple and effective and considerably reduces the count of the candidate VVs in the reduced control set.
2) The response of the reference VV-based methods for reducing the computation burden depends on the accuracy of the stator resistance. The proposed method does not require the stator resistance magnitude for the calculation of the CSC vector and the drive response is not affected by the changes in the stator resistance magnitude due to the temperature variation.
3) A new cost function without a weighting factor is introduced in this article, which directly compares the per-unit CSC vector with per-unit candidate VVs for selecting the optimal VV. With the introduction of the new cost function, the time-consuming stator current predictions for different candidate VVs are eliminated.
4) In the proposed scheme, the calculation complexity is reduced considerably due to the reduced control set and elimination of the current predictions, thereby causing a

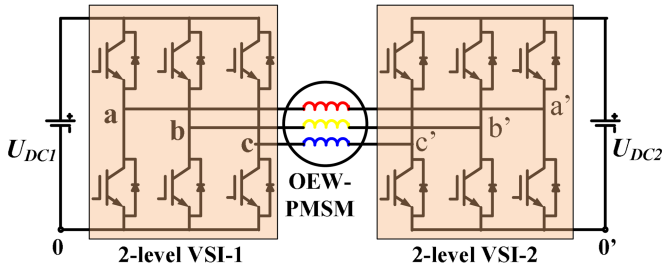

Fig. 1. Circuit topology for four-level inversion fed OEW-PMSM.

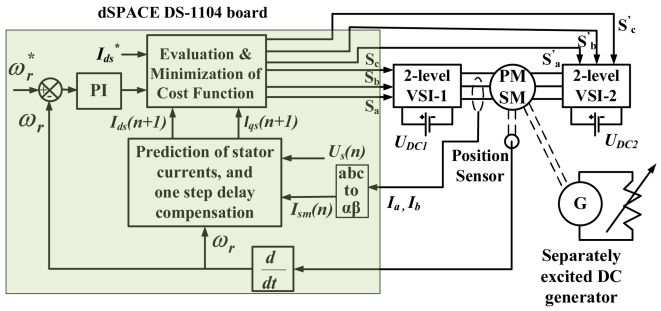

Fig. 2. Control diagram of MPCC of OEW-PMSM.

substantial reduction in the computation time of the MPCC algorithm.

This article is organized as follows. Section II presents the mathematical model of the OEW-PMSM. The conventional MPCC of the OEW-PMSM drive is discussed in Section III. Section IV explains the proposed MPCC of the OEW-PMSM drive. Experimental results are indicated and discussed in Section V. Finally, Section VI concludes this article.

II. Dynamic Model of PMSM

The topology of dual inverter fed OEW-PMSM is illustrated in Fig. 1. In this topology, two different two-level voltage source inverters (VSI) are used. The two VSI are fed with two isolated dc voltage sources ($U_{\rm DC1}$ and $U_{\rm DC2}$). To obtain four-level voltage across PMSM, the dc voltage magnitude of $U_{\rm DC1}$ and $U_{\rm DC2}$ is set in the ratio of 2:1 (i.e., $U_{\rm DC1} = 2U_{\rm DC}/3$ and $U_{\rm DC2} = U_{\rm DC}/3$). In this OEW-PMSM configuration, if each VSI is operated independently with eight different switching combinations, the pole voltages corresponding to each inverter are presented as per the following equations:

$$\begin{pmatrix} U_{a0} \\ U_{b0} \\ U_{c0} \end{pmatrix} = \left(\frac{2U_{\rm DC}}{3}\right) \begin{pmatrix} S_a \\ S_b \\ S_c \end{pmatrix} \tag{1}$$

$$\begin{pmatrix} U_{a'0'} \\ U_{b'0'} \\ U_{c'0'} \end{pmatrix} = \left(\frac{U_{\rm DC}}{3}\right) \begin{pmatrix} S_{a'} \\ S_{b'} \\ S_{c'} \end{pmatrix}. \tag{2}$$

The phase voltage across stator winding of OEW-PMSM is given by

$$\begin{pmatrix} U_{aa'} \\ U_{bb'} \\ U_{cc'} \end{pmatrix} = \begin{pmatrix} 2/3 & -1/3 & -1/3 \\ -1/3 & 2/3 & -1/3 \\ -1/3 & -1/3 & 2/3 \end{pmatrix} \begin{pmatrix} U_{a0} - U_{a'0'} \\ U_{b0} - U_{b'0'} \\ U_{c0} - U_{c'0'} \end{pmatrix}. \tag{3}$$

The stator voltage of PMSM in the stator reference frame is presented by

$$\overrightarrow{U_s} = \overrightarrow{I_s}\, R_s + L_s \frac{d\overrightarrow{I_s}}{dt} + j\overrightarrow{\psi_r}\omega_r \tag{4}$$

where $\overrightarrow{\psi_r} = \psi_r\, e^{j\theta_r}$, and R_s and L_s are the per-phase stator resistance and inductance of the PMSM. $\overrightarrow{U_s}$ and $\overrightarrow{I_s}$ are the space vectors of the stator voltage and stator current. The magnitude of the rotor flux linkages is ψ_r. ω_r and θ_r are the rotor speed in electrical rad/sec and rotor position angle in electrical radians, respectively.

From (4), the differential equation of d and q axes stator current in the rotor reference frame are presented by the following equations:

$$\frac{dI_{qs}}{dt} = \frac{1}{L_s} U_{qs} - \frac{R_s}{L_s} I_{qs} - \omega_r I_{ds} - \frac{\psi_r \omega_r}{L_s} \tag{5}$$

$$\frac{dI_{ds}}{dt} = \frac{1}{L_s} U_{ds} - \frac{R_s}{L_s} I_{ds} + \omega_r I_{qs} \tag{6}$$

where U_{ds} and U_{qs} are the d and q axes components of stator voltage space vector in the rotor reference frame. I_{ds} and I_{qs} are the d and q axes components of the stator current space vector in the rotor reference frame, respectively.

The speed-torque dynamics of the PMSM drive are presented by

$$\frac{d\omega_r}{dt} = \frac{P}{2J}\,(M_d - M_l) \tag{7}$$

where M_l is the load torque, J is the polar moment of inertia of the PMSM drive, P is the number of poles in the PMSM, and M_d is the torque produced by the PMSM and can be indicated by

$$M_d = \left(\frac{3}{2}\right)\left(\frac{P}{2}\right)\psi_r I_{qs}. \tag{8}$$

The above equations characterize the complete dynamic model of the OEW-PMSM drive fed with dual inverters having isolated dc sources.

III. Conventional MPCC of OEW-PMSM

The MPCC of four-level inversion fed OEW-PMSM is explained in this section. The control diagram of MPCC of OEW-PMSM is indicated in Fig. 2. The dual inverters are fed with the isolated dc voltage sources whose magnitudes are in the ratio of 2:1. In this configuration, 37 distinct VVs can be realized across the stator winding of the OEW-PMSM. The location of the voltage space vectors in the complex $\alpha\beta$–plane is shown in Fig. 3. These voltage space vectors along with their real and imaginary components are listed in Table I. In the MPCC of OEW-PMSM, the d and q axes stator currents are the basic control variables and there is no requirement for the estimation of the electromagnetic torque and stator flux. In PMSM, the electromagnetic torque is

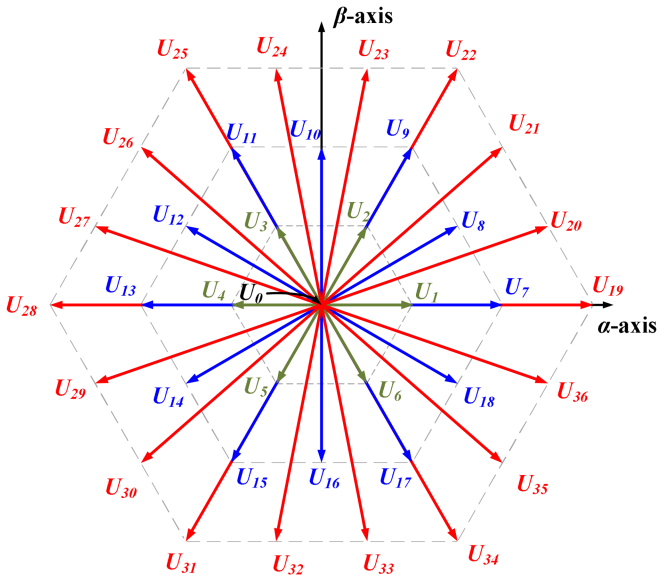

Fig. 3. Voltage space vectors for four-level inversion fed OEW-PMSM.

a function of the q-axis stator current. Therefore, the variations in the q-axis stator current produce proportional changes in the electromagnetic torque. The speed PI controller generates the reference for the q-axis stator current. Similarly, the changes in the d-axis stator current create proportional changes in the stator flux. The permanent magnets on the rotor are responsible for the generation of the flux. Therefore, the reference for the d-axis stator current is set to zero.

The dc voltage and stator currents are sensed and the space vectors for the stator voltage and stator current are found. The sampling of a signal and its analog to digital conversion involves a finite delay. Therefore, to compensate for the introduced delay, one-step delay compensation is performed.

The stator current space vector in the stator reference frame after one-step delay compensation can be represented by

$$\overrightarrow{I_s}\ (n) = \overrightarrow{I_{sm}}\ (n) + \frac{T_s}{L_s}\left(\overrightarrow{U_s}\,(n-1) - R_s\overrightarrow{I_{sm}}\,(n) - j\psi_r\omega_r\,(n)\,e^{j\theta_r}\right) \tag{9}$$

where $\overrightarrow{I_{sm}}$ is the stator current space vector found using the measured instantaneous stator currents. T_s is the sampling time and n is the sample number.

After delay compensation, both of the control variables (i.e., I_{ds} and I_{qs}) are predicted for 37 different VVs as per the following equations, which are obtained after discretizing (5) and (6) using the Euler's first-order approximation:

$$I_{ds}\ (n+1) = I_{ds}\ (n) + \frac{T_s}{L_s}\left(U_{ds} - I_{ds}\,(n)\,R_s + L_s I_{qs}\,(n)\,\omega_r\,(n)\right) \tag{10}$$

$$I_{qs}\ (n+1) = I_{qs}\ (n) + \frac{T_s}{L_s}\left(U_{qs} - I_{qs}\,(n)\,R_s - L_s I_{ds}\,(n)\,\omega_r\,(n) - \psi_r\omega_r\,(n)\right). \tag{11}$$

TABLE I
VVs FOR FOUR-LEVEL INVERSION FED OEW-PMSM

Space Vector U_s	VSI-1 Switching State (S_a,S_b,S_c)	VSI-2 Switching State (S'_a,S'_b,S'_c)	$U_{\alpha s}$	$U_{\beta s}$
U_0	(0, 0, 0)	(0, 0, 0)	0	0
U_1	(0, 0, 0)	(0, 1, 1)	$(2/9)U_{DC}$	0
U_2	(0, 0, 0)	(0, 0, 1)	$(1/9)U_{DC}$	$(\sqrt{3}/9)\,U_{DC}$
U_3	(0, 0, 0)	(1, 0, 1)	$(-1/9)U_{DC}$	$(\sqrt{3}/9)\,U_{DC}$
U_4	(0, 0, 0)	(1, 0, 0)	$(-2/9)U_{DC}$	0
U_5	(0, 0, 0)	(1, 1, 0)	$(-1/9)U_{DC}$	$(-\sqrt{3}/9)\,U_{DC}$
U_6	(0, 0, 0)	(0, 1, 0)	$(1/9)U_{DC}$	$(-\sqrt{3}/9)\,U_{DC}$
U_7	(1, 0, 0)	(1, 1, 1)	$(4/9)U_{DC}$	0
U_8	(1, 0, 0)	(1, 0, 1)	$(1/3)U_{DC}$	$(\sqrt{3}/9)\,U_{DC}$
U_9	(1, 1, 0)	(1, 1, 1)	$(2/9)U_{DC}$	$(2\sqrt{3}/9)\,U_{DC}$
U_{10}	(0, 1, 0)	(0, 1, 1)	0	$(2\sqrt{3}/9)\,U_{DC}$
U_{11}	(0, 1, 0)	(1, 1, 1)	$(-2/9)U_{DC}$	$(2\sqrt{3}/9)\,U_{DC}$
U_{12}	(0, 1, 0)	(1, 1, 0)	$(-1/3)U_{DC}$	$(\sqrt{3}/9)\,U_{DC}$
U_{13}	(0, 1, 1)	(1, 1, 1)	$(-4/9)U_{DC}$	0
U_{14}	(0, 0, 1)	(1, 0, 1)	$(-1/3)U_{DC}$	$(-\sqrt{3}/9)\,U_{DC}$
U_{15}	(0, 0, 1)	(1, 1, 1)	$(-2/9)U_{DC}$	$(-2\sqrt{3}/9)\,U_{DC}$
U_{16}	(0, 0, 1)	(0, 1, 1)	0	$(-2\sqrt{3}/9)\,U_{DC}$
U_{17}	(1, 0, 1)	(1, 1, 1)	$(2/9)U_{DC}$	$(-2\sqrt{3}/9)\,U_{DC}$
U_{18}	(1, 0, 0)	(1, 1, 0)	$(1/3)U_{DC}$	$(-\sqrt{3}/9)\,U_{DC}$
U_{19}	(1, 0, 0)	(0, 1, 1)	$(2/3)U_{DC}$	0
U_{20}	(1, 0, 0)	(0, 0, 1)	$(5/9)U_{DC}$	$(\sqrt{3}/9)\,U_{DC}$
U_{21}	(1, 1, 0)	(0, 1, 1)	$(4/9)U_{DC}$	$(2\sqrt{3}/9)\,U_{DC}$
U_{22}	(1, 1, 0)	(0, 0, 1)	$(1/3)U_{DC}$	$(\sqrt{3}/3)\,U_{DC}$
U_{23}	(1, 1, 0)	(1, 0, 1)	$(1/9)U_{DC}$	$(\sqrt{3}/3)\,U_{DC}$
U_{24}	(0, 1, 0)	(0, 0, 1)	$(-1/9)U_{DC}$	$(\sqrt{3}/3)\,U_{DC}$
U_{25}	(0, 1, 0)	(1, 0, 1)	$(-1/3)U_{DC}$	$(\sqrt{3}/3)\,U_{DC}$
U_{26}	(0, 1, 0)	(1, 0, 0)	$(-4/9)U_{DC}$	$(2\sqrt{3}/9)\,U_{DC}$
U_{27}	(0, 1, 1)	(1, 0, 1)	$(-5/9)U_{DC}$	$(\sqrt{3}/9)\,U_{DC}$
U_{28}	(0, 1, 1)	(1, 0, 0)	$(-2/3)U_{DC}$	0
U_{29}	(0, 1, 1)	(1, 1, 0)	$(-5/9)U_{DC}$	$(-\sqrt{3}/9)\,U_{DC}$
U_{30}	(0, 0, 1)	(1, 0, 0)	$(-4/9)U_{DC}$	$(-\sqrt{3}/9)\,U_{DC}$
U_{31}	(0, 0, 1)	(1, 1, 0)	$(-1/3)U_{DC}$	$(-\sqrt{3}/3)\,U_{DC}$
U_{32}	(0, 0, 1)	(0, 1, 0)	$(-1/9)U_{DC}$	$(-\sqrt{3}/3)\,U_{DC}$
U_{33}	(1, 0, 1)	(1, 1, 0)	$(1/9)U_{DC}$	$(-\sqrt{3}/3)\,U_{DC}$
U_{34}	(1, 0, 1)	(0, 1, 0)	$(1/3)U_{DC}$	$(-\sqrt{3}/9)\,U_{DC}$
U_{35}	(1, 0, 1)	(0, 1, 1)	$(4/9)U_{DC}$	$(-2\sqrt{3}/9)\,U_{DC}$
U_{36}	(1, 0, 0)	(0, 1, 0)	$(1/3)U_{DC}$	$(-\sqrt{3}/9)\,U_{DC}$

A cost function (X), defined by (12), is evaluated for every pair of predicted currents, and the VV, which minimizes the cost function, is selected as the optimal VV. The selected optimal VV is applied across the OEW-PMSM in the next sampling interval.

$$X = \left|I^*_{ds} - I_{ds}\,(n+1)\right| + \left|I^*_{qs} - I_{qs}\,(n+1)\right|. \tag{12}$$

In 4-level inversion fed MPCC operated OEW-PMSM, 37 prediction calculations of d-q axes current, corresponding to every available VV, take place in each sampling interval. The prediction process in the conventional MPCC is time-consuming and puts a heavy burden on the digital processor. Because of this reason, there is a minimum limit on the selection of the sampling period.

IV. PROPOSED MPCC OF OEW-PMSM

An MPCC-operated 4-level inversion fed OEW-PMSM requires 37 predictions of d-q axes currents in every sampling interval. Each of the 37 available VVs is considered for the

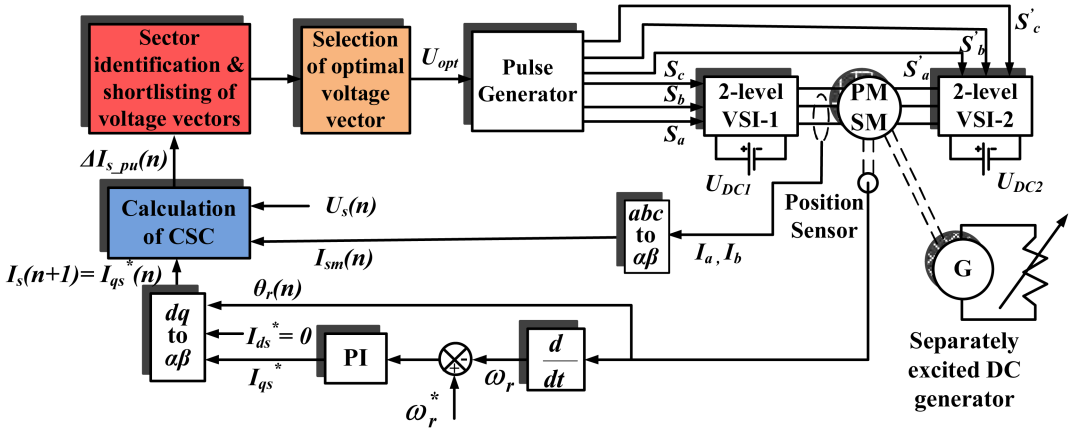

Fig. 4. Control diagram of proposed MPCC of OEW-PMSM.

prediction of the currents. The prediction process is time-consuming and places a heavy burden on the digital processor. This also puts a minimum limit on the selection of the sampling period. In the proposed MPCC, the number of calculations is significantly reduced, thereby achieving an extensive drop in the computation burden of the digital processor. In the proposed scheme, the computations are reduced in two steps. In the first step, the count of VVs used for the predictions is reduced and up to four VVs are shortlisted for the modified control set. The space vector of CSC is calculated. The magnitude and direction of the CSC vector are used for obtaining the reduced control set. In the second step, the complex predictions of the control variables are eliminated and the VV from the reduced control set which is nearer to the CSC space vector is selected as an optimal VV.

The control diagram for the proposed MPCC fed OEW-PMSM is shown in Fig. 4. The circuit structure of the proposed scheme is the same as that of a conventional four-level inversion fed OEW-PMSM. The control technique for the proposed MPCC is explained in steps and contains two parts: 1) shortlisting of VVs for the proposed control set and 2) selection of optimal VV.

A. Shortlisting of Voltage Vectors (VV) for the Proposed Control Set

The active VVs produced by the dual inverters include 6 small vectors, 12 medium vectors, and 18 large vectors. In this article, the count of VVs is reduced from 37 to a maximum of 4. The space vector for the stator current at the *n*th sampling instant is found from the sensed currents and one-step delay compensation. The error between the reference and the actual speed is processed by the speed PI controller to generate the reference magnitude for the *q*-axis stator current. Maximum torque per ampere (MTPA) of the stator current is achieved for the PMSM by continuously having the *d*-axis stator current as zero. During MTPA, the *q*-axis stator current is varied to produce the required torque. Therefore, the reference *q*-axis stator current (I_{qs}^*) is selected as the current for the next sampling interval. The magnitude of I_{qs}^* is obtained from the speed PI controller.

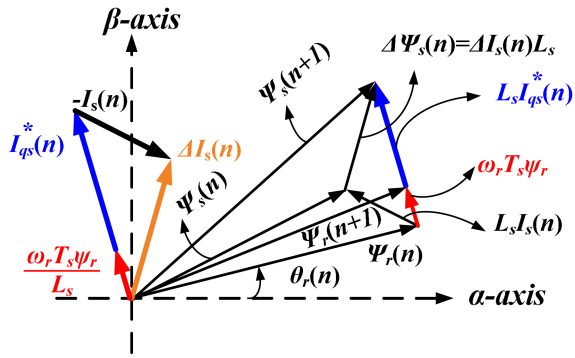

Fig. 5. Phasor diagram of the proposed MPCC-controlled PMSM.

The phasor diagram of the proposed MPCC-controlled PMSM is shown in Fig. 5. The change in the rotor flux angle in one sampling interval is $\omega_r T_s$. As the change in the angle of rotor flux is very small, the magnitude of the change in the rotor flux space vector in one sampling interval is approximately given by

$$\left|\overrightarrow{\Delta\psi_r}\right| = \psi_r \ \sin\left(\omega_r T_s\right) \cong \omega_r T_s \psi_r. \tag{13}$$

The direction of the vector for the change in the rotor flux $\overrightarrow{\Delta\psi_r}$ is perpendicular to $\overrightarrow{\psi_r}(n)$. In one sampling interval, the position of the rotor flux vector is shifted. From Fig. 5 and (13), the rotor flux vector for the $(n+1)$th sampling instant is given by

$$\overrightarrow{\psi_r}\ (n+1) = \overrightarrow{\psi_r}\ (n) + \overrightarrow{\Delta\psi_r}. \tag{14}$$

For a surface PMSM, the space vector of stator flux in the stationary reference frame is found from the following equation:

$$\overrightarrow{\psi_s}\ (n) = L_s\ \overrightarrow{I_s}\ (n) + \overrightarrow{\psi_r}\ (n)\,. \tag{15}$$

Similarly, from Fig. 5, the stator flux space vector for the $(n+1)$th sampling instant is given by

$$\overrightarrow{\psi_s}\ (n+1) = L_s \left[I_{qs}^*\ (n) + \frac{\omega_r T_s \psi_r}{L_s}\right] e^{j\left(\theta_r(n)+\frac{\pi}{2}\right)} + \overrightarrow{\psi_r}\ (n)\,. \tag{16}$$

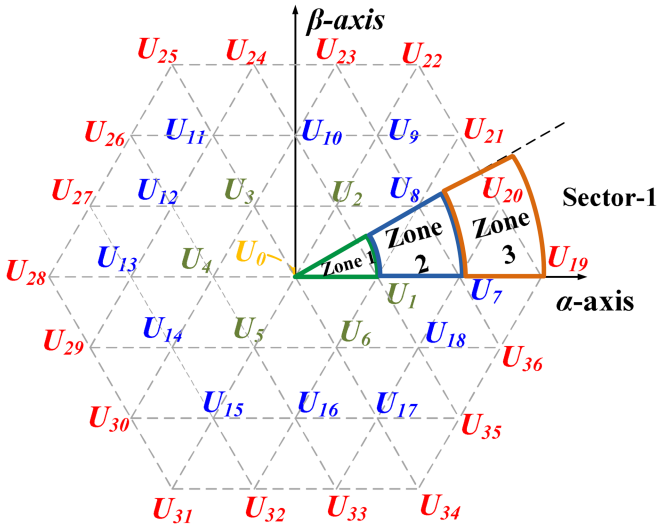

Fig. 6. Shortlisting of VVs for control set of proposed MPCC.

The change in the stator flux vector in one sampling interval ($\overrightarrow{\Delta\psi_s}$) can be obtained by subtracting (15) from (16) and given by the following equations

$$\overrightarrow{\Delta\psi_s}\ (n) = \left[\left(I_{qs}^{*}\,(n) + \frac{\omega_r T_s \psi_r}{L_s}\right) e^{j\left(\theta_r(n)+\frac{\pi}{2}\right)} - \overrightarrow{I_s}\,(n)\right] L_s \tag{17}$$

$$\overrightarrow{\Delta\psi_s}\ (n) = \overrightarrow{\Delta I_s}\ (n)\, L_s \tag{18}$$

where $\overrightarrow{\Delta I_s}(n)$ is the CSC calculated at the nth sample. $\overrightarrow{\Delta I_s}(n)$ is given by

$$\overrightarrow{\Delta I_s}\ (n) = \left[I_{qs}^{*}\,(n) + \frac{\omega_r T_s \psi_r}{L_s}\right] e^{j\left(\theta_r(n)+\frac{\pi}{2}\right)} - \overrightarrow{I_s}\,(n)\,. \tag{19}$$

Since the stator flux changes in the direction of the applied VV, the optimal VV is nearer to the space vector of $\overrightarrow{\Delta\psi_s}(n)$. Also, from the (18), it is clear that the CSC vector $\overrightarrow{\Delta I_s}(n)$ is in the direction of $\overrightarrow{\Delta\psi_s}(n)$. Therefore, the direction of the CSC vector is used for the selection of the candidate VV of the reduced control set. In the proposed scheme, the complex $\alpha\beta$-plane is divided into 12 equal sectors. Sector 1 is defined between 0° and 30°. Similarly, 11 other sectors of 30° span are defined. Each of the 12 sectors is divided into 3 zones at equal intervals (i.e., zone 1, zone 2, and zone 3) as indicated in Fig. 6. The VVs indicated in Fig. 6 are the per-unit vectors, which are obtained after dividing their original magnitude by $\frac{2}{3}U_{\mathrm{DC}}$. Similarly, the per-unit CSC vector is obtained from

$$\overrightarrow{\Delta I_s^{pu}}\ (n) = \frac{\overrightarrow{\Delta I_s}\,(n)}{\Delta I_s^{\max}\,(n)} \tag{20}$$

where

$$\Delta I_s^{\max}\ (n) = \frac{2U_{\mathrm{DC}}T_s}{3L_s}\,.$$

TABLE II
VOLTAGE VECTORS FOR THE REDUCED CONTROL SET OF THE PROPOSED MPCC

Sector Number	Zone1	Zone2	Zone3
1	(U_0, U_1)	(U_1, U_7, U_8)	$(U_7, U_8, U_{19}, U_{20})$
2	(U_0, U_2)	(U_2, U_8, U_9)	$(U_8, U_9, U_{21}, U_{22})$
3	(U_0, U_2)	(U_2, U_9, U_{10})	$(U_9, U_{10}, U_{22}, U_{23})$
4	(U_0, U_3)	(U_3, U_{10}, U_{11})	$(U_{10}, U_{11}, U_{24}, U_{25})$
5	(U_0, U_3)	(U_3, U_{11}, U_{12})	$(U_{11}, U_{12}, U_{25}, U_{26})$
6	(U_0, U_4)	(U_4, U_{12}, U_{13})	$(U_{12}, U_{13}, U_{27}, U_{28})$
7	(U_0, U_4)	(U_4, U_{13}, U_{14})	$(U_{13}, U_{14}, U_{28}, U_{29})$
8	(U_0, U_5)	(U_5, U_{14}, U_{15})	$(U_{14}, U_{15}, U_{30}, U_{31})$
9	(U_0, U_5)	(U_5, U_{15}, U_{16})	$(U_{15}, U_{16}, U_{31}, U_{32})$
10	(U_0, U_6)	(U_6, U_{16}, U_{17})	$(U_{16}, U_{17}, U_{33}, U_{34})$
11	(U_0, U_6)	(U_6, U_{17}, U_{18})	$(U_{17}, U_{18}, U_{34}, U_{35})$
12	(U_0, U_1)	(U_1, U_7, U_{18})	$(U_7, U_{18}, U_{19}, U_{36})$

The angle of the CSC vector is used to select the sector number in which it is located. The VVs are shortlisted for the reduced control set from the sector number and the zone number. The radial width of each zone is 0.33 units. If the per-unit CSC vector has a magnitude between 0 and 0.33, then zone 1 will be selected. If the per-unit CSC vector has a magnitude between 0.33 and 0.66, then zone 2 will be selected. Similarly, if the per-unit CSC vector has a magnitude between 0.66 and 1, then zone 3 will be selected. Table II indicates the candidate VVs for the reduced control set, as per the sector and zone in which the CSC vector is located. The first zone selects two VVs for the reduced control set, whereas zone 2 and zone 3 select, respectively, three and four VVs.

B. *Selection of Optimal Voltage Vector (VV)*

The reduced control set of the proposed MPCC includes a maximum of four per-unit VVs. In the proposed control scheme, the prediction of the control variables (i.e., I_{ds} and I_{qs}) for different candidate VVs is absent. A new cost function (G) is introduced in the proposed scheme. The cost function contains the absolute value of the vector difference between the per-unit CSC vector and the per-unit candidate VV. The per-unit CSC vector is compared with each of the per-unit candidate VV of the reduced control set. The VV that minimizes the cost function G is selected as an optimal VV (U_{opt})

$$G = \left|\overrightarrow{\Delta I_s^{pu}}\,(n) - \overrightarrow{U_k^{p}}\,(n+1)\right| \tag{21}$$

where $\overrightarrow{U_k^{p}}(n+1)$ is the per-unit candidate VV of the reduced control set for the next sampling interval which is given by

$$\overrightarrow{U_k^{p}}\ (n+1) = \frac{\overrightarrow{U_k}\,(n+1)}{2U_{\mathrm{DC}}/3}. \tag{22}$$

A flowchart for the proposed method is shown in Fig. 7. The selected optimal VV also minimizes the error between the reference and the actual d-q axes stator currents. The effect of the introduced cost function and the selected optimal VV, on the stator currents, is the same as that of conventional MPCC. The conventional 4-level inversion fed MPCC of OEW-PMSM

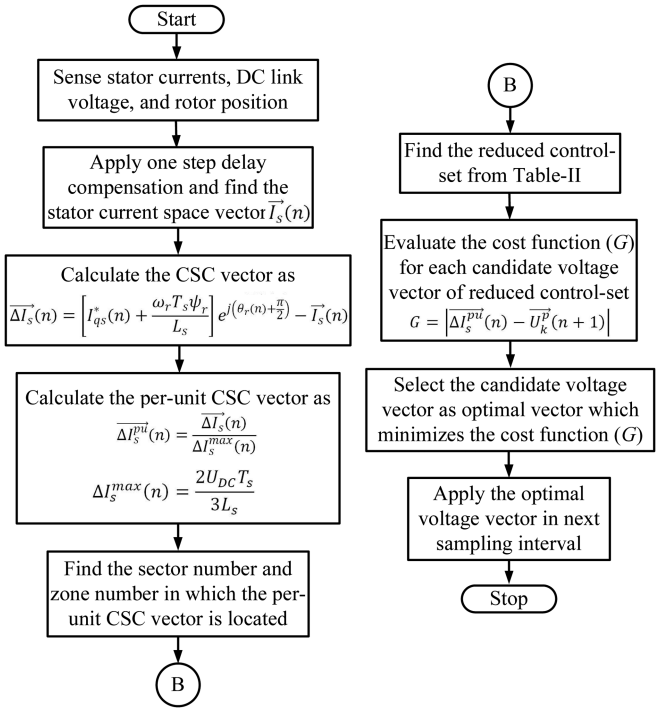

Fig. 7. Flowchart for proposed MPCC of OEW-PMSM.

TABLE III
PMSM AND CONTROL PARAMETERS

Parameter	Value
Stator winding resistance	1.12 Ω
Stator winding inductance	0.0105 H
Rated speed	1500 r/min
Rated RMS voltage	415 V
Permanent magnet flux	0.7 Wb
Number of rotor poles	4
Sampling time	150 μs

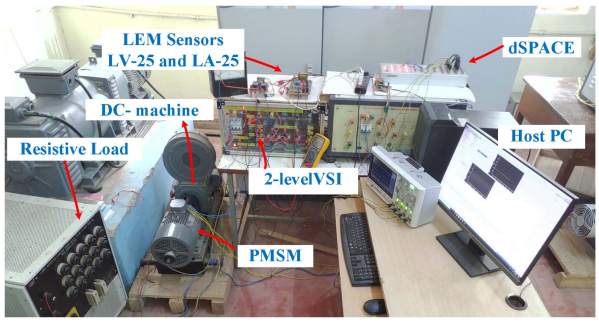

Fig. 8. Experimental arrangement of the drive and the control hardware.

uses 37 VVs for the prediction of the stator currents. In the proposed MPCC-operated OEW-PMSM, the candidate VVs are shortlisted from 37 to a maximum 4, using the location of CSC vector in the complex $\alpha\beta$–plane. With I_{qs}^* as the predicted current, the CSC vector is proportional to the required change in the stator flux. Any VV produces the change in the stator flux in the same direction as that VV. Therefore, the CSC vector is used for shortlisting the candidate VVs of the reduced control set. The proposed cost function selects an optimal VV nearer to the per-unit CSC vector. The selected VV, when applied for the next sampling interval brings the stator current nearer to the reference current. The conventional MPCC and the proposed MPCC minimize the error between the reference current and the actual current in every sampling interval. The proposed method selects the optimal VV with considerably fewer computations.

V. EXPERIMENTAL RESULTS

The proposed scheme using a reduced control set is experimentally tested and compared with the conventional MPCC and the MPCC of the OEW-PMSM as presented in [19], i.e., MPCC [19]. The results obtained in the experimental testing are analyzed and discussed in this section. The parameters of the PMSM used for experimentation are listed in Table III. The OEW-PMSM is fed through two two-level inverters with each inverter connected to an isolated dc voltage source. The PMSM is loaded through a coupled dc generator connected to the variable resistive load. The dc-link voltage and the stator currents are sensed by the Hall effect sensors. The position of the rotor is sensed through a 1024 point incremental encoder. dSPACE DS-1104 is used for the implementation of the control logic. A sampling time of 150 μs is used in the experiment for both the control methods. To obtain a fair comparison, the gains of the PI controllers are kept unchanged while testing each control scheme. The experimental arrangement of the drive and the control hardware is shown in Fig. 8.

In the beginning, the steady state response from the OEW-PMSM is obtained at 400, 800, and 1400 rev/min with 35% loading. The steady-state response of the torque, stator flux, current and speed is plotted through a digital storage oscilloscope. Fig. 9 shows the steady-state response of OEW-PMSM drive with each of the considered control methods. It can be observed from the steady-state response of the PMSM that the peak-to-peak torque ripple and flux ripple generated by the PMSM is almost equal at every speed. No variation in the steady-state performance of the proposed scheme was shown and the drive operates with the identical torque and flux ripples as in the conventional MPCC with 37 VVs and MPCC [19]. The OEW-PMSM is tested under the transient conditions of the speed reversal and step change in the load. The response of the OEW-PMSM under a transient state is plotted using a digital storage oscilloscope. The dynamic response of the OEW-PMSM, when controlled with each of the considered methods, is shown in Fig. 10. For both control methods, the speed reversal is performed from −500 to 500 rev/min at no load. It can be seen from the transient response of Fig. 10, that the conventional MPCC, MPCC [19] and the proposed MPCC take identical time (0.45 s) to reverse the speed of the PMSM.

A step change in the load from 0 to 5 N·m at 1000 rev/min is applied to the PMSM when controlled with each control method. PMSM takes around 0.4 s to supply the applied load in each

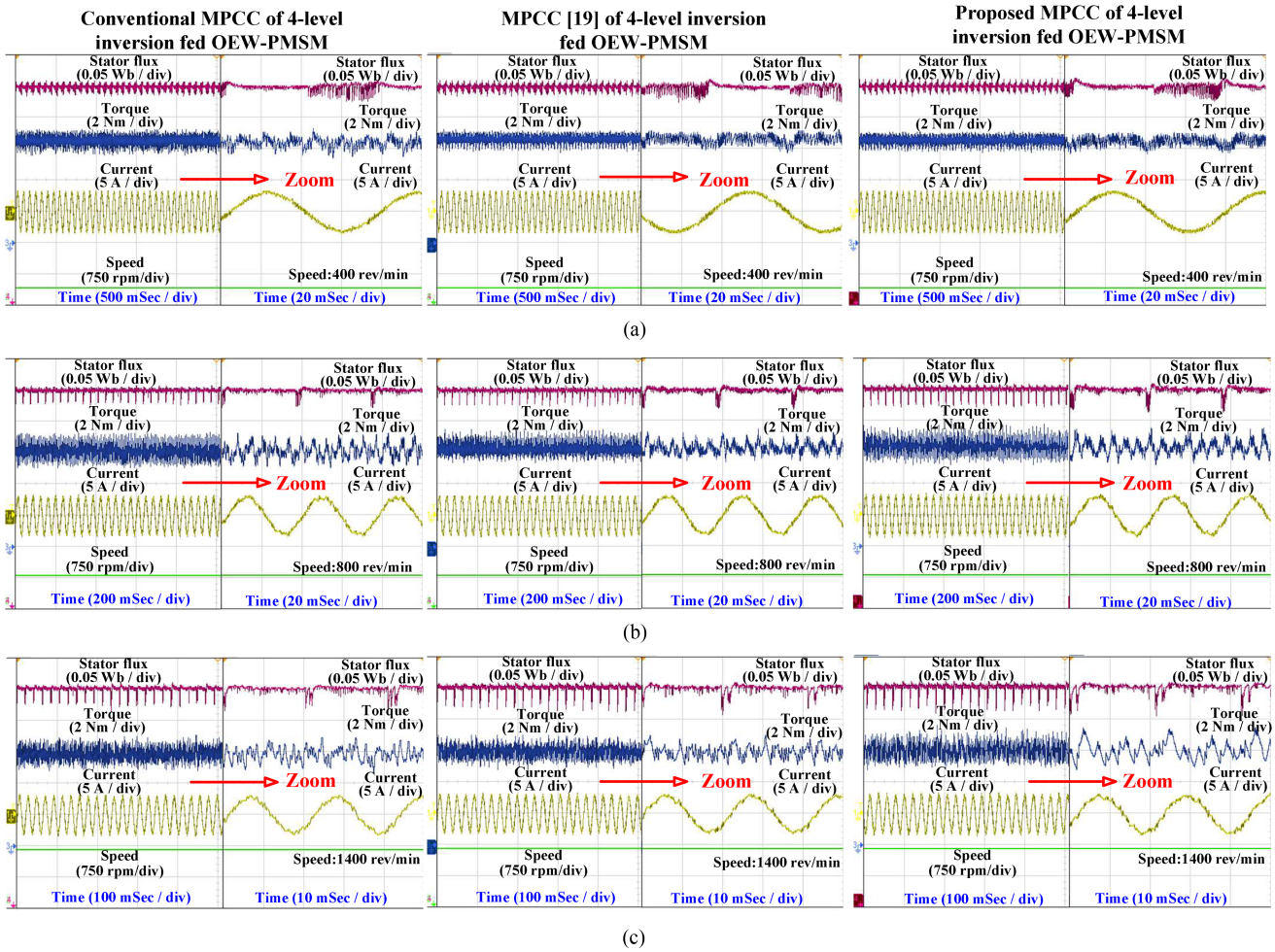

Fig. 9. Steady-state response of conventional, MPCC [19] and proposed MPCC operated four-level inversion fed OEW-PMSM drive at (a) 400 rev/min, (b) 800 rev/min, and (c) 1400 rev/min.

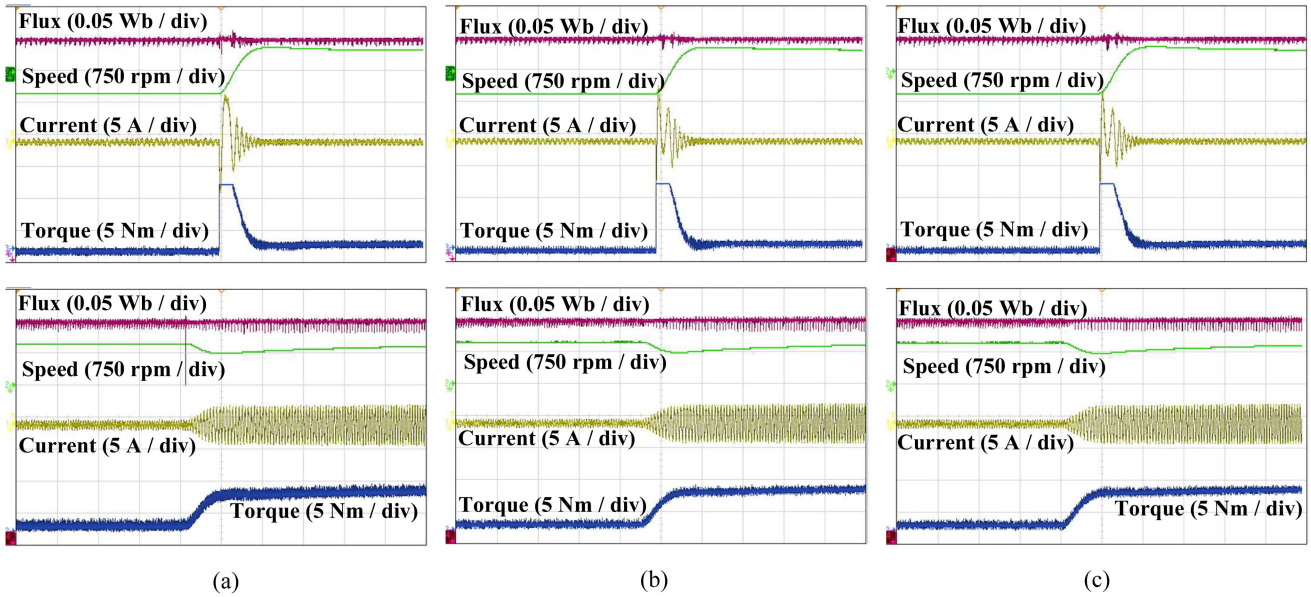

Fig. 10. Dynamic response during speed reversal and step change in the load for (a) conventional MPCC, (b) MPCC [19], and (c) proposed MPCC operated four-level inversion fed OEW-PMSM drive (time scale: 500 ms/div).

TABLE IV
COMPARISON BETWEEN CONVENTIONAL MPCC, MPCC [16], MPCC [19], AND PROPOSED MPCC

	Conventional MPCC	MPCC[16]	MPCC[19]	Proposed MPCC
Variables used in reducing the vector count	No reduction in the vector count	Torque error and Sector information of stator flux vector	Sector information of the reference voltage VV	Magnitude and sector information of CSC vector
Count of voltage vectors in reduced control set	37	16	9	2−4
Percentage reduction in the turnaround time	No reduction	29	43	55
Steady state response	Unchanged	Unchanged	Unchanged	Unchanged
Control variables used in the cost function	Stator d-q axes current	Stator flux, torque and x-y axes current	$\alpha\beta 0$-axes stator voltages	Per-unit CSC and stator voltage
Dependency on the PMSM parameters	R_s, L_s, and ψ_r	R_s, L_s, and ψ_r	R_s, L_s, and ψ_r	L_s and ψ_r

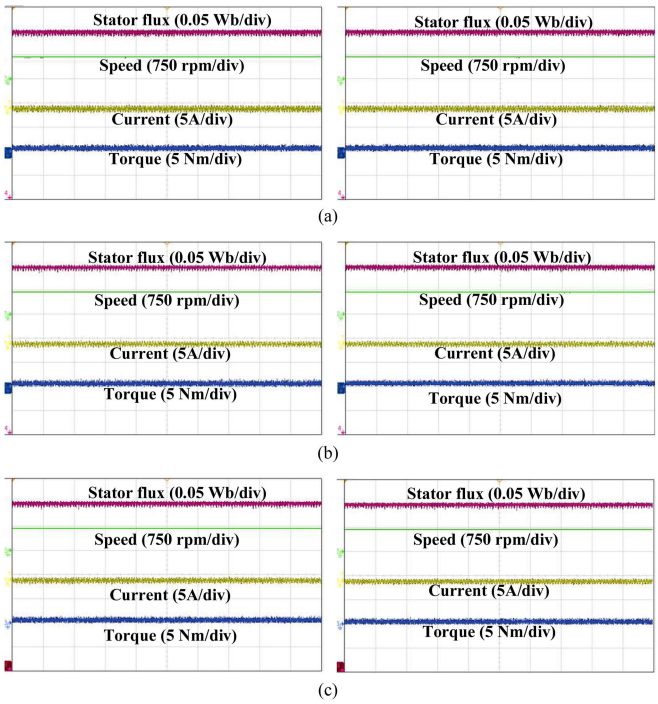

Fig. 11. Steady-state response of OEW-PMSM without change in the parameters (left) and with 15% increased parameters (right) for (a) conventional MPCC, (b) MPCC [19], and (c) proposed MPCC.

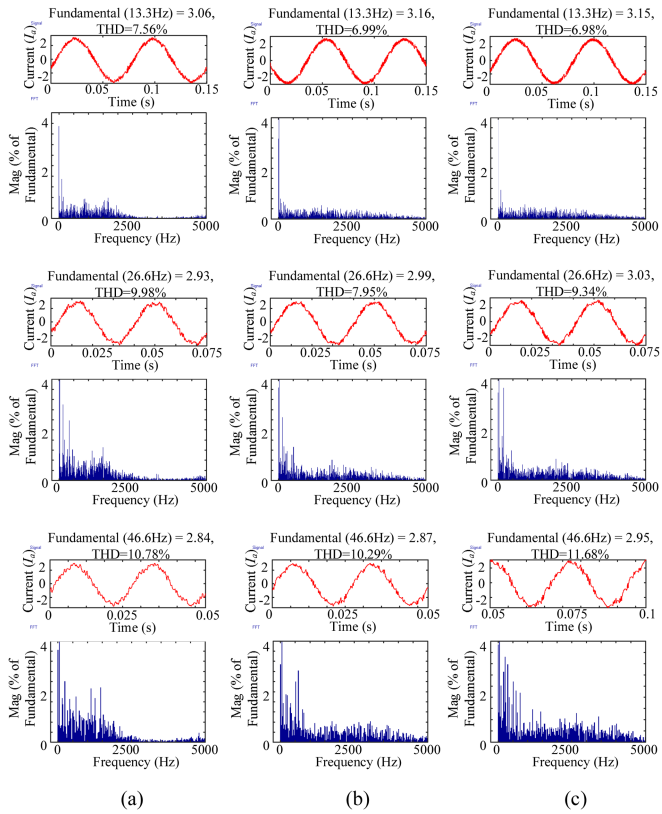

Fig. 12. Frequency spectrum of stator current at 400, 800, and 1400 r/min for (a) conventional MPCC, (b) MPCC [19], and (c) proposed MPCC.

control scheme. It is clear that both the control methods have shown similar dynamic responses and there is no change in the response times.

The PMSM drive is tested for parameter sensitivity when operating with the conventional MPCC, MPCC [19] and the proposed MPCC schemes. The stator inductance and the rotor flux linkages are disturbed with a 15% increment. The steady-state response at 700 rev/min is obtained with and without parameter variations of the PMSM. The obtained results for the parameter sensitivity are indicated in Fig. 11. It is clear from Fig. 11 that for the control methods with 15% parameter variation, the PMSM has shown a very minor deviation in the response. Therefore, the OEW-PMSM drive operates robustly when controlled with the proposed MPCC. The harmonic spectrum of the stator current at different speeds is obtained and indicated in Fig. 12. The percentage of total harmonic distortion (THD) in the stator current of the proposed MPCC is almost identical when compared to the conventional MPCC and MPCC [19]. A comparison between conventional MPCC, MPCC [16], MPCC [19], and the proposed MPCC is tabulated in Table IV. The computation time is measured for the conventional MPCC, MPCC [19] and the proposed MPCC-operated OEW-PMSM and the average value is calculated. The average execution time for the control methods

TABLE V
EXECUTION TIME FOR CONVENTIONAL MPCC, MPCC [19], AND PROPOSED MPCC ON DSPACE DS-1104 CONTROLLER

Control Method	Execution Time
Conventional MPCC using 37 vectors	128.6 μS
MPCC [19]	74.13 μS
Proposed MPCC	57.25 μS

implemented on the dSPACE DS-1104 controller is shown in Table V. The execution time for the proposed scheme is reduced by almost 55% and 12% when compared to the conventional MPCC and MPCC [19] respectively. The proposed MPCC is less time-consuming and it is possible to implement it on a processor with less computation power.

VI. CONCLUSION

This article has proposed a simple predictive current control scheme for a four-level inversion fed OEW-PMSM to lower the computation burden on the processor. The proposed technique has successfully reduced the number of VVs in the control set from the original 37 to a maximum 4. The shortlisting of the VVs is obtained by using the location of the per-unit CSC vector. The per-unit CSC vector is in the direction of the vector for the required change in the stator flux with q-axis stator current as the next sample current. The proposed cost function successfully selects the optimal VV. With the elimination of the predictions of the stator currents for different VVs and with the implementation of a simple cost function, the proposed algorithm's complexity is considerably reduced. With the CSC vector as the selection criterion for the candidate VV and with the proposed cost function, the error in the stator current is minimized similar to the conventional MPCC. In the experimentation, the PMSM drive is successfully tested with conventional MPCC using 37 VVs, MPCC [19], and the proposed MPCC using a maximum of 4 VVs. The different responses obtained during the experimental testing of each of the methods are identical. However, with the proposed scheme, the computation burden on the processor is lowered by 55% and 12% when compared to the conventional MPCC and MPCC [19]. With the successful reduction in the computation time, it is possible to implement the proposed MPCC scheme using a lower sampling period.

REFERENCES

[1] F. Mendoza-Mondragón, V. M. Hernández-Guzmán, and J. Rodríguez-Reséndiz, "Robust speed control of permanent magnet synchronous motors using two-degrees-of-freedom control," *IEEE Trans. Ind. Electron.*, vol. 65, no. 8, pp. 6099–6108, Aug. 2018.

[2] P. Kakosimos and H. Abu-Rub, "Predictive speed control with short prediction horizon for permanent magnet synchronous motor drives," *IEEE Trans. Power Electron.*, vol. 33, no. 3, pp. 2740–2750, Mar. 2018.

[3] J. A. Güemes, A. M. Iraolagoitia, J. I. Del Hoyo, and P. Fernández, "Torque analysis in permanent-magnet synchronous motors: A comparative study," *IEEE Trans. Energy Convers.*, vol. 26, no. 1, pp. 55–63, Mar. 2011.

[4] D. Q. Dang, M. S. Rafaq, H. H. Choi, and J.-W. Jung, "Online parameter estimation technique for adaptive control applications of interior PM synchronous motor drives," *IEEE Trans. Ind. Electron.*, vol. 63, no. 3, pp. 1438–1449, Mar. 2016.

[5] Q. An, J. Liu, Z. Peng, L. Sun, and L. Sun, "Dual-space vector control of open end winding permanent magnet synchronous motor drive fed by dual inverter," *IEEE Trans. Power Electron.*, vol. 31, no. 12, pp. 8329–8342, Dec. 2016.

[6] A. P. Sandulescu, F. Meinguet, X. Kestelyn, E. Semail, and A. Bruyere, "Flux-weakening operation of open-end winding drive integrating a cost-effective high-power charger," *IET Electr. Syst. Transp.*, vol. 3, no. 1, pp. 10–21, Mar. 2013.

[7] A. D. Kiadehi, K. E. K. Drissi, and C. Pasquier, "Voltage THD reduction for dual-inverter fed open-end load with isolated DC sources," *IEEE Trans. Ind. Electron.*, vol. 64, no. 3, pp. 2102–2111, Mar. 2017.

[8] A. Edpuganti and A. K. Rathore, "New optimal pulsewidth modulation for single DC-link dual-inverter fed open end stator winding induction motor drive," *IEEE Trans. Power Electron.*, vol. 30, no. 8, pp. 4386–4393, Aug. 2015.

[9] M. Chen and D. Sun, "A unified space vector pulse width modulation for dual two-level inverter system," *IEEE Trans. Power Electron.*, vol. 32, no. 2, pp. 889–893, Feb. 2017.

[10] B. V. Reddy, V. T. Somasekhar, and Y. Kalyan, "Decoupled space-vector PWM strategies for a four-level asymmetrical open-end winding induction motor drive with waveform symmetries," *IEEE Trans. Ind. Electron.*, vol. 58, no. 11, pp. 5130–5141, Nov. 2011.

[11] M. R. Baiju, K. K. Mohapatra, R. S. Kanchan, and K. Gopakumar, "A dual two-level inverter scheme with common mode voltage elimination for an induction motor drive," *IEEE Trans. Power Electron.*, vol. 19, no. 3, pp. 794–805, May 2004.

[12] C. Bordons and C. Montero, "Basic principles of MPC for power converters: Bridging the gap between theory and practice," *IEEE Ind. Electron. Mag.*, vol. 9, no. 3, pp. 31–43, Sep. 2015.

[13] K. Eshwar and V. K. Thippiripati, "Weighting-factorless predictive torque control scheme for dual inverter fed open-end-winding PMSM with single DC source," *IEEE Trans. Power Electron.*, vol. 36, no. 11, pp. 12968–12978, Nov. 2021.

[14] M. Siami, D. A. Khaburi, M. Rivera, and J. Rodríguez, "A computationally efficient lookup table based FCS-MPC for PMSM drives fed by matrix converters," *IEEE Trans. Ind. Electron.*, vol. 64, no. 10, pp. 7645–7654, Oct. 2017.

[15] T. Geyer, "Computationally efficient model predictive direct torque control," *IEEE Trans. Power Electron.*, vol. 26, no. 10, pp. 2804–2816, Oct. 2011.

[16] M. S. H. Sabbir and M. Habibullah, "Selective voltage vector based predictive torque control of five-phase induction motor drive," in *Proc. 11th Int. Conf. Electr. Comput. Eng.*, 2020, pp. 182–185.

[17] B. Zhu, K. Rajashekara, and H. Kubo, "A novel predictive current control for open-end winding induction motor drive with reduced computation burden and enhanced zero sequence current suppression," in *Proc. IEEE Appl. Power Electron. Conf. Expo.*, 2017, pp. 552–557.

[18] K. M. R. Eswar, K. V. P. Kumar, and T. V. Kumar, "A simplified predictive torque control scheme for open-end winding induction motor drive," *IEEE J. Emerg. Sel. Topics Power Electron.*, vol. 7, no. 2, pp. 1162–1172, Jun. 2019.

[19] M. S. R. Saeed, W. Song, B. Yu, Z. Xie, and X. Feng, "Low-complexity deadbeat model predictive current control for open-winding PMSM drive with zero-sequence current suppression," *IEEE Trans. Transp. Electrific.*, vol. 7, no. 4, pp. 2671–2682, Dec. 2021.

[20] Y. Luo and C. Liu, "A flux constrained predictive control for a six-phase PMSM motor with lower complexity," *IEEE Trans. Ind. Electron.*, vol. 66, no. 7, pp. 5081–5093, Jul. 2019.

[21] S. Niu, Y. Luo, W. Fu, and X. Zhang, "An indirect reference vector-based model predictive control for a three-phase PMSM motor," *IEEE Access*, vol. 8, pp. 29435–29445, 2020.

[22] M. Mamdouh and M. A. Abido, "Efficient predictive torque control for induction motor drive," *IEEE Trans. Ind. Electron.*, vol. 66, no. 9, pp. 6757–6767, Sep. 2019.

[23] T. Tao, W. Zhao, Y. Du, Y. Cheng, and J. Zhu, "Simplified fault-tolerant model predictive control for a five-phase permanent-magnet motor with reduced computation burden," *IEEE Trans. Power Electron.*, vol. 35, no. 4, pp. 3850–3858, Apr. 2020.

[24] C. Sun, D. Sun, W. Chen, and H. Nian, "Improved model predictive control with new cost function for hybrid-inverter open-winding PMSM system based on energy storage model," *IEEE Trans. Power Electron.*, vol. 36, no. 9, pp. 10705–10715, Sep. 2021.

[25] Y. Wang et al., "Fast response model predictive torque and flux control with low calculation effort for PMSMs," *IEEE Trans. Ind. Inform.*, vol. 15, no. 10, pp. 5531–5540, Oct. 2019.

Sagar Gajanan Petkar was born in Nashik, India, in 1985. He received the B.E. degree in electrical engineering from Pune University, Pune, India, in 2007, and the M.Tech. degree in electrical engineering from the Indian Institute of Technology, Bombay, Mumbai, India, in 2010. He is currently working toward the Ph.D. degree with the Electrical Engineering Department, National Institute of Technology, Warangal, Warangal, India.

From 2011 to 2018, he was an Assistant Professor with Pune University. His research interests include power electronics, high-performance electrical drives, direct torque control, and model predictive control.

Vinay Kumar Thippiripati (Senior Member, IEEE) was born in Kadapa, India, in 1984. He received the B.Tech. and M.Tech. degrees from Jawaharlal Nehru Technological University, Hyderabad, Hyderabad, India, in 2005 and 2008, respectively, and the Ph.D. degree from the National Institute of Technology, Warangal, Warangal, India, in 2015.

In 2013, he joined the National Institute of Technology, Warangal, as an Assistant Professor. His research interests include power electronics and drives, direct torque control, predictive torque control, open-end winding induction motor drives, multilevel inverters, hybrid electric vehicles, and renewable energy interfacing.